MDPI

Article

Spherical ZVI/Mn-C Bimetallic Catalysts for Efficient Fenton-like Reaction under Mild Conditions

Lu Qin [1],[†], Xin Yu [1],[†], Kang Wang [2],* and Xitao Wang [1],*

[1] Tianjin Key Laboratory of Applied Catalysis Science and Technology, School of Chemical Engineering and Technology, Tianjin University, Tianjin 300072, China; qinlu_tju@163.com (L.Q.); a17803871784@163.com (X.Y.)

[2] Tianjin Key Laboratory of Membrane Science and Desalination Technology, Chemical Engineering Research Center, College of Chemical Engineering and Technology, Tianjin University, Tianjin 300072, China

* Correspondence: wangk72@tju.edu.cn (K.W.); wangxt@tju.edu.cn (X.W.); Tel.: +86-155-2289-3935 (K.W.); +86-138-2015-0137 (X.W.)

[†] These authors contributed equally to this work.

Abstract: The heterogeneous Fenton-like reaction has been receiving increasing attention for its inexpensiveness and high efficiency in water treatment. In this study, a novel strategy was proposed for preparing spherical ZVI/Mn-C bimetallic catalysts with a high activity for a Fenton-like reaction by using the ammonium alginate assisted sol–gel method coupled with a carbothermic reduction. The results showed that the obtained ZVI/Mn-C spheres had a uniform size, smooth surface and good sphericity, and the particle size of ZVI was limited to about 30 nm by the carbon layer. Among all catalysts, the ZVI/Mn-C-31 catalyst exhibited the highest phenol degradation efficiency in the Fenton-like process, and almost 100% phenol degradation efficiency was achieved under neutral pH at room temperature within 5 min. Moreover, the ZVI/Mn-C-31/H_2O_2 system showed a 100% degradation efficiency for removing a wide range of aromatic pollutants, including catechol, resorcinol and o-nitrophenol. Moreover, the radicals-scavenging experiment illustrated that the ·OH played a key factor in mineralizing the organic matters, and the ·O_2^- generated from the MnO-H_2O_2 system accelerated the conversion rate of ferric iron to ferrous iron. Due to the synergistic effects between ZVI and MnO, the ZVI/Mn-C-31 catalyst performed excellently in the Fenton-like reaction at an extended pH range.

Keywords: Fenton-like reaction; PF-derived carbon spheres; ZVI; manganous oxide

1. Introduction

The increasing contamination of water poses a serious threat to human health and sustainable development. As one of the common phenolic compounds in water pollution, phenol is toxic to human and aquatic life, even at very low concentrations [1]. Various techniques including biotechnology [2], photocatalysis [3], electrocatalysis [4], adsorption [5] and advanced oxidation [6] have been developed to remove phenol from wastewater. The Fenton-like reaction, as one of the most promising advanced oxidation processes, has been widely used in the removal of phenol due to its high efficiency and environmental friendliness [7]. With the hydroxyl radicals involved, most organic pollutants can be efficiently mineralized into CO_2 and H_2O [8–10]. However, obvious drawbacks existed for the homogeneous Fenton reaction such as a low activity at higher pH and the secondary pollution owing to the iron sludge [11,12], which limited its application and prospect. To solve these problems, many advances have been achieved including the heterogeneous Fenton reaction, the fluidized bed Fenton reaction and the electro-Fenton reaction [13–16]. Among these approaches, the heterogeneous Fenton reaction has attracted the most attention for its inexpensiveness and high efficiency.

Fe/C coupled materials have been considered to be effective catalysts for the heterogeneous Fenton reaction, and the synergistic effects between Fe and carbon species on

Fe species dispersion, organic matter adsorption, H_2O_2 activation and electron transfer have been studied widely [17–21]. Carbon materials, such as carbon nanotubes (CNTs), graphene oxide (GO) and activated carbon (AC), have been used to immobilize iron species within the surface and pores, which exhibited a distinctive reactivity of the Fenton-like reaction. Li et al. [22] constructed an Fe_3O_4/carbon catalyst derived from an iron-based metal organic framework for degrading methylene blue (MB). The carbon carrier not only provided a porous and stable layer for Fe_3O_4 but acted as a ·OH generator when reacting with hydrogen peroxide. In recent years, the research of zero valent iron (ZVI) and its application in heterogeneous Fenton processes have attracted considerable attention due to its eco-friendliness, inexpensiveness and high reactivity [23–25]. The oxidation ability of zero-valent iron is generally considered to be more than seven times that of iron ions, which makes it an effective agent for reducing various environmental pollutants in wastewater [26]. However, the reactivity of ZVI in heterogeneous Fenton processes has usually been limited by its dispersion. Chen et al. [27] synthesized ZVI/C composites from commercial iron oxide and graphite, for which ibuprofen-containing wastewater was completely degraded by ZVI/C in 4 h with the presence of H_2O_2. Moreover, the leaching concentration of iron ions in the solution was only 4.8 mg L^{-1} after reaction, which demonstrated the high activity and stability of ZVI/C composites. The introduction of carbon materials solved the problem of ZVI agglomeration and was conducive to the synthesis of nanoscale ZVI. Du et al. [28] utilized biochar as a carbon source to synthesize ZVI/C composites by a one-step carbothermic reduction method. No agglomeration of ZVI was observed due to the large specific surface area of the AC carrier. Although these studies have shown a significant high efficiency of ZVI/C composites, the practical application of ZVI/C composites has been seriously hindered with the consideration of their inherent defects, such as their high cost, difficulty in separation and harsh reaction conditions. In addition, a higher activity for the Fenton-like reaction was achieved when iron species coupled with other transition metals [29–33]. The Cu-Fe/ZrO_2 system was applied to a heterogeneous Fenton process for the mineralization of ibuprofen [30]. Due to the presence of Cu and ZrO_2, this system displayed the highest mineralization ratio (83%) of ibuprofen under the condition of pH = 3. However, the mineralization ratio abruptly dropped to 10% in a neutral environment. Specifically, manganese species have been widely used in catalysts due to their low cost, abundant mineral resources, high catalytic activity and multivalent properties. Manganese species could extend the applicable pH range of iron-based catalysts, making the reaction maintain a high efficiency even under neutral conditions [10,34–36]. Sun et al. [35] reported a novel Mn^{2+}-mediated Fenton-like process based on an Fe(III)-NTA complex that was superefficient at a circumneutral pH range. The degradation rate constant of crotamiton, a model compound, by the Fe(III)-NTA Mn^{2+} Fenton-like process was at least 1.6 orders of magnitude larger than that in the absence of Mn^{2+}. Other metal ions such as Ca^{2+}, Mg^{2+}, Co^{2+} and Cu^{2+} had no impacts or little inhibitory effect on the Fe(III)-NTA-complex-catalyzed Fenton-like reaction. Moses G et al. [37] synthesized Mn-Fe/SiO_2 bimetallic catalysts for the heterogeneous Fenton degradation of methylene blue, with 97% of the dye degraded at near neutral pH. Unfortunately, the reaction rate of this catalyst was limited by silica spheres due to the lack of pore structure, and it is difficult to effectively mineralize organic pollutants.

In view of the above problems, the phenol resin (PF)-based carbon spheres with a millimeter scale, smooth surface and high sphericity are more competitive for heterogeneous Fenton processes due to its facile preparation and ease of separation. According to a previous paper [38], spherical activation carbon with a diameter of about 2 mm can be prepared by an ammonium alginate (ALG)-assisted sol–gel method using PF as the carbon precursor, which can be applied to the preparation of a spherical ZVI/Mn-C bimetallic catalyst. The prepared ZVI/Mn-C catalysts showed the following advantages: (1) it is facile and effective to introduce the metals with uniform dispersion into the carbon spheres via a carbothermic method; (2) the synergistic effect of ZVI and Mn species immobilized on activated carbon could be helpful to achieve a higher activity and extend the pH range

in the heterogeneous Fenton reaction; (3) the reacted ZVI/Mn-C catalysts could be easily separated from wastewater. Herein, in this work, five ZVI/Mn-C samples with different ratios of Fe^{3+}/Mn^{2+} were synthesized, characterized and tested in the degradation of phenol and chemical oxygen demand (COD). The synergistic effect between ZVI and MnO on the degradation efficiency of phenol were investigated, and a reaction mechanism was proposed according to the radicals-scavenging experiments. The as-prepared ZVI/Mn-C catalysts exhibited a high efficiency for phenol and COD removal, leading to a novel method for the catalyst to treat toxic organic wastewater at neutral conditions.

2. Results and Discussion

2.1. Characterization of Catalysts

In this work, the ammonium alginate (ALG) containing an abundant carboxyl group was used as the forming agent of spherical ZVI/Mn-C samples, which possessed a higher activity to coordinate with metal ions. As shown in Figure 1, the chelating reaction between Fe^{3+}/Mn^{2+} and the carboxyl group in ALG occurred when the mixture of PF, PE and ALG was dropped into an Fe^{3+}/Mn^{2+} solution with a syringe, and an Fe^{3+}/Mn^{2+}-alginate gel with a three-dimensional network structure was formed. Figure 1 also shows the optical photographs of the PF-derived carbon spheres prepared via the alginate-assisted method. The wet samples showed a uniformly spherical shape with a smooth surface, and the average diameter was about 4 mm. After being calcined in a nitrogen atmosphere at 850 °C, no obvious change in the morphology and the degree of sphericity could be seen, but the particle size shrank significantly to about 2–3 mm due to the removal of water. The mechanical strength and average pore diameters of all samples are listed in Table 1. The mechanical strength of ZVI/Mn-C-11 was highest at 17.5 N/bead, which can prevent the spherical catalyst from cracking during the entire reaction process. In addition, the average pore size of all samples was 3–4 nm in mesopore size, which was consistent with previously reported results [38].
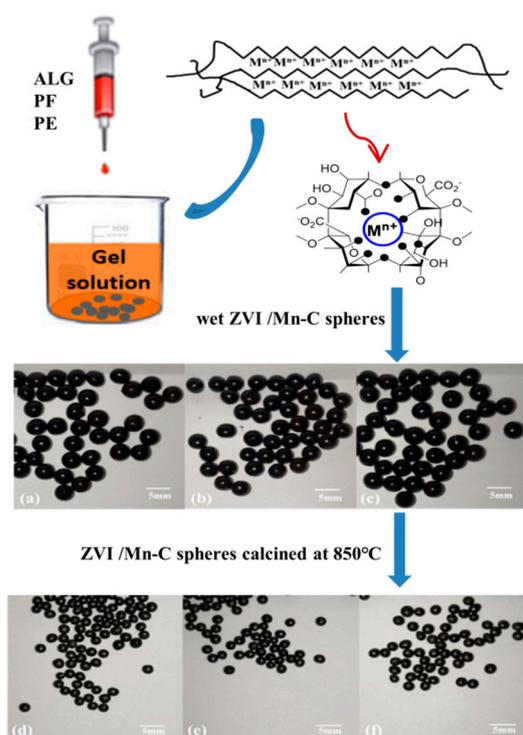

Figure 1. Schematic diagram of the preparation process for (**a,d**) ZVI/Mn-C-31, (**b,e**) ZVI/Mn-C-11, (**c,f**) ZVI/Mn-C-13.

Table 1. Ultimate mechanical strength and average pore diameter of all samples.

Sample	ZVI-C	ZVI/Mn-C-31	ZVI/Mn-C-11	ZVI/Mn-C-13	Mn-C
Mechanical strength (N·bead^{-1})	6.5	12.3	17.5	13.3	8.9
Average pore diameter (nm)	3.409	3.399	3.855	4.154	4.144

The XRD patterns of ZVI/Mn-C samples are shown in Figure 2. The Mn-C sample displayed diffraction peaks at 40.5°, 58.7°, 70.2° and 73.8°, which were ascribed to the (200), (220), (311) and (222) crystal planes of the cubic MnO phase (JCPDS no. 772363), indicating that MnO could not be reduced to Mn metal during the carbothermic reduction. For the ZVI-C sample, diffraction peaks at 44.6° and 65.2° attributed to the (110) and (200) crystal planes of ZVI (JCPDS no. 87-0721) were detected, demonstrating that ferric iron was converted into ZVI by the carbothermic reduction. With the introduction of manganese species, the XRD peaks of ZVI became gradually weak, indicating a good dispersion of ZVI. A diffraction peak indexed to MnO could not be seen among the ZVI/Mn-C samples, which can be due to the isomorphic substitution between iron and manganese atoms just as reported in a previous paper [34]. Meanwhile, the structures of the ZVI/Mn-C composites were further investigated by their Raman spectra and the result was a shown in Figure 3. The weak peaks around 640 cm^{-1} were attributed to the stretching vibration of the Mn-O bond in MnO [39–41], proving the existence of manganese oxide in the ZVI/Mn-C composites. In addition, the strong peaks at 1341 and 1581 cm^{-1} were ascribed to the disordered carbon (D-band) and the ordered graphitic carbon (G-band) in the PF-derived carbon spheres, respectively. From the Raman spectra, the intensity ratios of the D and G bands of ZVI/Mn-C samples were 2.89, 2.33, 2.67, 2.60 and 1.54 for ZVI-C, ZVI/Mn-C-31, ZVI/Mn-C-11, ZVI/Mn-C-13 and Mn-C, respectively. All the ZVI/Mn-C samples were rich in disordered carbon but lacking in graphitic carbon, especially with the existence of iron.
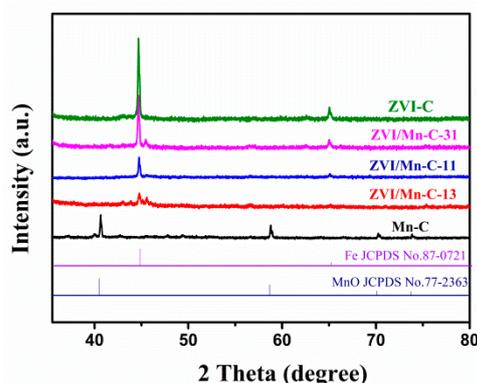
Figure 2. XRD patterns of ZVI/Mn-C samples.

The morphology of the as-prepared samples was examined by TEM, as shown in Figure 4. It can be clearly seen that the spherical-shaped ZVI nanoparticles were embedded in the active carbon. The size of the ZVI particles in ZVI-C and ZVI/Mn-C-31 was about 30 nm (Figure 4a–c), which was much smaller than those ever reported in the literature [42–44], illustrating that the alginate-assisted method can effectively inhibit the agglomeration of ZVI. Furthermore, the lattice spacing of 0.20 nm was observed in the HRTEM image of the ZVI/Mn-C-31 catalyst, which was assigned to the (110) plane of ZVI (Figure 4d). In addition, small MnO particles with a fine nanostructure and uniform dispersion on a carbon matrix can be found (Figure 4e). The spacing of the clear lattice fringes in Figure 4f was found to be 0.22 nm, which was coincident with the (200) d-value of MnO. In addition, the

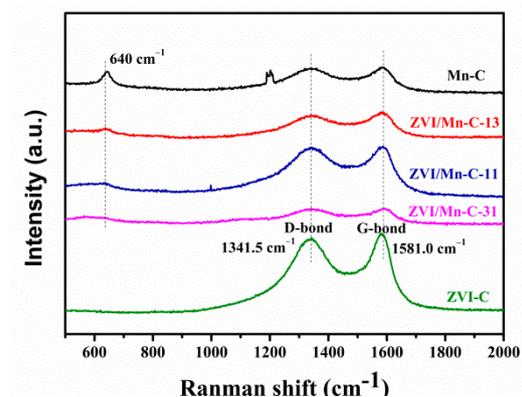selected area electron diffraction (SAED) patterns of the Mn-C sample also matched well with typical MnO [45].
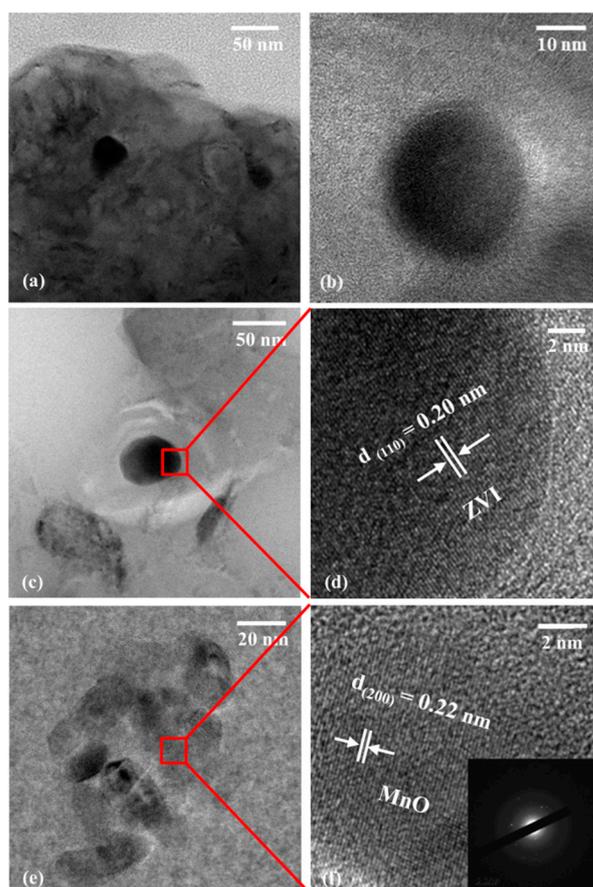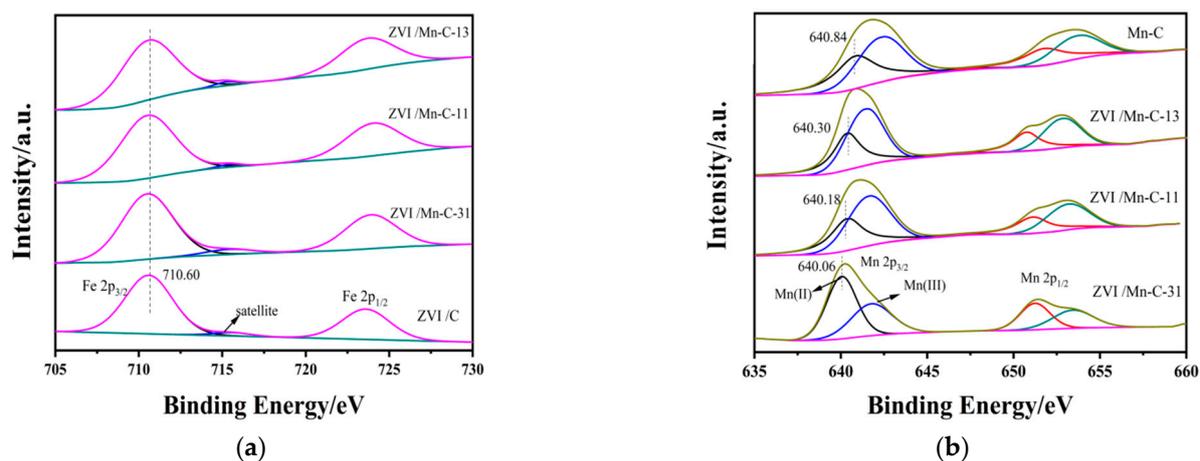

Figure 3. Raman spectra of ZVI/Mn-C samples.

Figure 4. TEM images of (**a**,**b**) ZVI-C, (**c**) ZVI/Mn-C-31 and (**e**) Mn-C; HRTEM image of (**d**) ZVI/Mn-C-31 and (**f**) Mn-C. The inset in (**f**) shows the SAED pattern of Mn-C.

An XPS characterization was carried out to investigate the composition and element chemical state in the obtained ZVI/Mn-C samples. As seen in Figure 5a, the peak at 710.60 eV of the four iron-containing samples was assigned to Fe $2p_{3/2}$ (Fe(III)), with its satellite signal at 715.5 eV [46]. No peak belonging to ZVI was detected in the spectra. These fitting results suggested that iron species on the surface were oxidized to Fe (III) by oxygen in the air. As shown in Figure 5b, the peaks in Mn 2p spectrum were attributed to

Mn (II) and Mn (III). Moreover, the presence of Mn (III) was also due to the partial oxidation by oxygen in the air. Compared to the monometallic Mn-C sample, the binding energy of Mn $2p_{3/2}$ shifted to a lower level with the incorporation of ZVI, which meant that ZVI acted as a good electron donor here. For the three bimetallic samples, the binding energy of Mn (II) $2p_{3/2}$ [47,48] shifted from 640.30 eV to 640.06 eV when the Fe/Mn ratio changed from 1:3 to 3:1. The results illustrated that the electron cloud density of the Mn species was higher with the increasing Fe/Mn ratios [49], which were consistent with the degradation results in this heterogeneous Fenton-like process.


Figure 5. XPS spectra of (**a**) Fe 2p and (**b**) Mn 2p for all samples.

2.2. Catalytic Activity

The catalytic performance of the ZVI/Mn-C samples was studied in the liquid-phase degradation of phenol under mild conditions. To reveal the real catalytic effect of the catalyst for phenol removal, comparative experiments were also carried out, and the phenol removal rate turned out to be 15.0% for ZVI/Mn-C-31 without the addition of hydrogen peroxide and 12.7% for hydrogen peroxide without catalysts after 4 h. As shown in Figure 6, the phenol was completely removed within only 5 min by three bimetallic ZVI/Mn-C catalysts. In addition, more than 50% of the COD was removed after 4 h in the reactions driven by the bimetallic catalysts, which demonstrated a high mineralization efficiency in this process. Meanwhile, the catalytic performance of the Mn-C and ZVI-C was also evaluated. The single metal catalysts exhibited relatively lower activity in the Fenton-like reaction, in which the degradation rate of phenol and COD were below 50% and 15% within 4 h, respectively. The result of the catalytic activity of ZVI was consistent with previous studies. The catalytic activity of ZVI was higher under acidic conditions, and the degradation efficiency was relatively low under mild conditions [50,51]. It was obvious that the degradation efficiency can be evidently promoted by the synergistic effect of ZVI and MnO. Moreover, the molar ratio of Fe^{3+}/Mn^{2+} had a significant effect on the Fenton-like reaction. The sample of ZVI/Mn-C-31 showed superior activity both of phenol and COD removal, and the COD removal rate reached 71.4% after 4 h. The synergy effect between ZVI and Mn was discussed in detail in Section 2.3. Therefore, the molar ratio of $Fe^{3+}:Mn^{2+} = 3:1$ was selected as the optimal value in this experiment.

In the heterogeneous Fenton-like reaction, the operating conditions affect the degradation efficiency of organic pollutants [51,52]. Firstly, the effect of the initial pH of the solution on the phenol removal over the ZVI/Mn-C-31 catalyst is shown in Figure 7a,b. No obvious difference existed for phenol removal over the extended pH range from 4 to 8, and the phenol was completely removed in 5 min. Notably, ZVI/Mn-C-31 exhibited a superior catalytic performance at pH = 7, and the conversion of COD was nearly 70% within 240 min. However, it was observed that the removal efficiency of phenol decreased greatly at an initial pH = 9. The inactivation was due to the decomposition of H_2O_2 at

alkaline conditions, which would seriously reduce the utilization of free radicals [52]. This illustrated that free radicals may be formed by the introduction of Mn, which enabled the ZVI/Mn-C-31 to have excellent catalytic performance in a wide pH range.

(**a**)

(**b**)
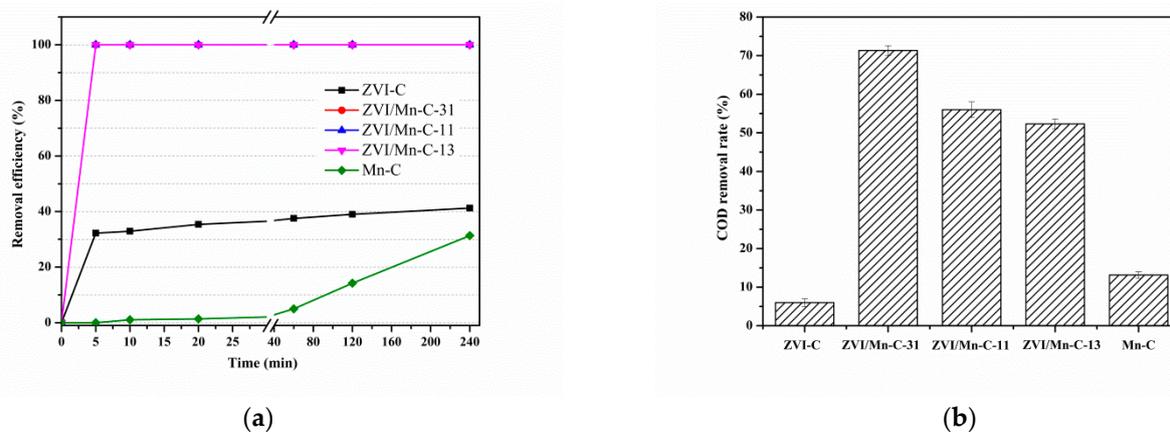
Figure 6. Effect of Fe/Mn molar ratio on (**a**) the degradation of phenol and (**b**) COD removal (Conditions: [ZVI/Mn-C] = 2 g/L, [phenol] = 100 mg/L, [H_2O_2] = 0.2 mol/L, initial pH = 7).


(**a**)

(**b**)

(**c**)

(**d**)
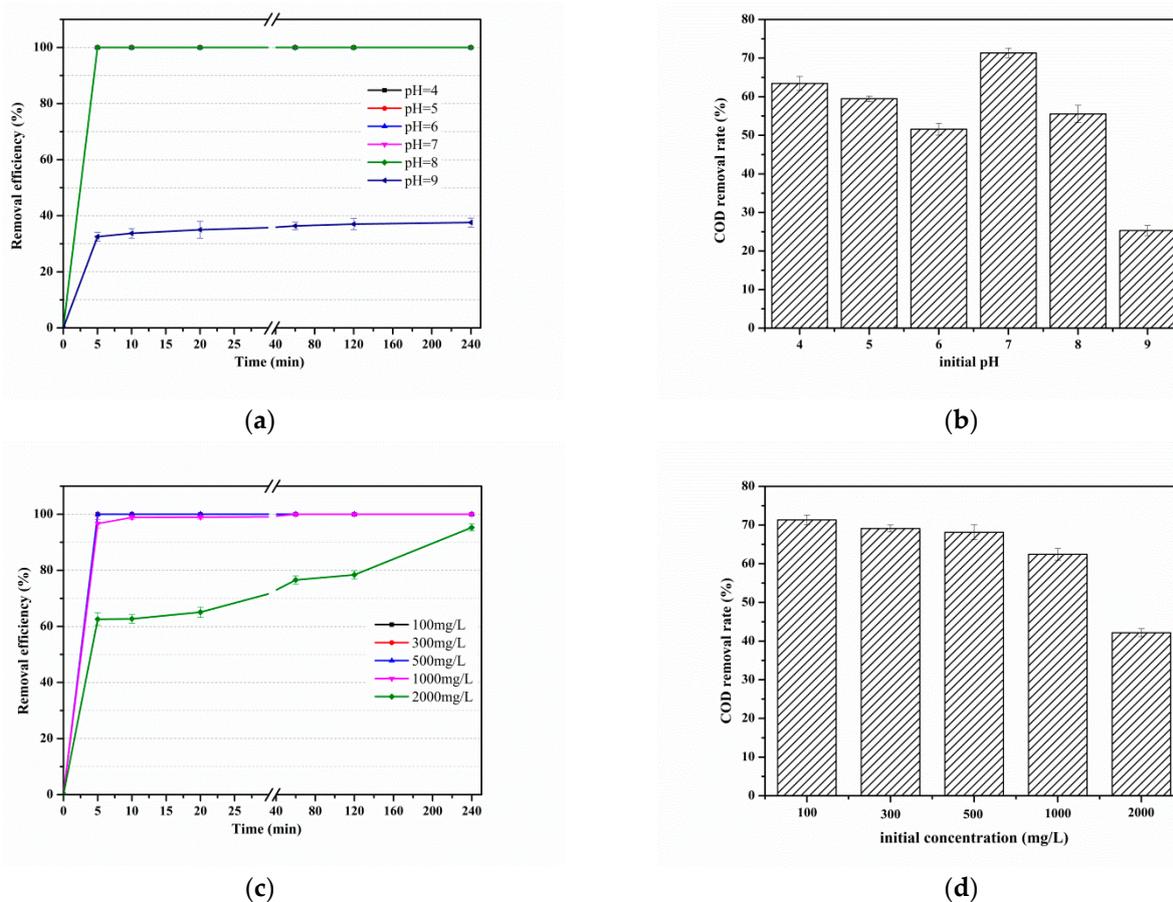
Figure 7. Influence of the operating conditions on the phenol removal in the Fenton-like reaction over the ZVI/Mn-C-31 catalyst. Effect of pH on (**a**) the degradation of phenol and (**b**) COD removal (conditions: [ZVI/Mn-C-31] = 2 g/L, [phenol] = 100 mg/L, [H_2O_2] = 0.2 mol/L). Effect of initial phenol concentration on (**c**) the degradation of phenol and (**d**) COD removal (conditions: [ZVI/Mn-C-31] = 2 g/L, [H_2O_2] = 0.2 mol/L, initial pH = 7).

The catalytic property of ZVI/Mn-C-31 to degrade phenol upon various initial concentration of phenol was evaluated. As seen in Figure 7c,d, the superior degradation rate of phenol and COD reached 100% and 71.4%, respectively. There was little influence of the initial concentration on phenol COD removal when the initial concentration of phenol varied from 100 mg/L to 500 mg/L. The removal rates of phenol and COD were decreased to approximately 90% and 62% by the Fenton-like process for 1000 mg/L. With a further increase of pollutant concentration to 2000 mg/L, the phenol removal efficiency was decreased to 59% and the COD removal rate dropped to 43%. It meant that ZVI and MnO could no longer generate sufficient free radicals under the presence of H_2O_2 at a higher initial concentration of phenol, thus reducing the degradation rate of phenol and COD. The result could be attributed to the competitive adsorption between the phenol and H_2O_2 on the active sites of the catalyst, which restrained the generation of radicals [53,54]. Compared with the results of previous studies for the phenol removal listed in Table 2, the prepared ZVI/Mn-C-31 catalyst exhibited a good phenol degradation efficiency and COD removal efficiency in the Fenton-like reaction. In addition, the initial reaction rates for the phenol removal over the ZVI/Mn-C-31 catalyst, expressed as per gram of the catalyst, were $0.05\ g_{phenol}/(min.\ g_{cat})$ at room temperature, respectively, under neutral pH in a 10 min reaction process. At the lower temperature (room temperature), the ZVI/Mn-C-31 catalyst had a higher reaction rate under neutral pH compared to that of the dendritic Fe^0 catalyst $(0.025\ g_{phenol}/(min.\ g_{cat}))$ under the acidic operating condition (pH = 4) [55]. The result proved that the ZVI/Mn-C-31 catalyst exhibited good performance in the Fenton-like reaction for the phenol degradation under a neutral pH.

Table 2. Comparison of various catalysts employed for phenol degradation via heterogeneous Fenton-like reaction.

Catalysts	Operating Conditions	Performance	References
ZVI/Mn-C-31	[Catalyst] = 2 g/L; [H_2O_2] = 0.2 M; [phenol] = 1 g/L, pH = 7.0; room temperature	Phenol removal: 100% (10 min) COD removal: 64% (240 min)	this work
Fe/Mn-MOF-71	[Catalyst]: 0.064 g/L; [H_2O_2]: 0.15 M; [Phenol]: 1 g/L; pH: 6.2; T: 35 °C	Phenol removal: 100% (120 min) COD removal: 43% (180 min)	[34]
$Fe_8O_8(OH)_{4\cdot5}(SO_4)_{1\cdot75}$	[Catalyst]: 1 g/L; [H_2O_2]: 14.70 mM; [Phenol]: 100 mg/L; pH: 3.0; room temperature	Phenol removal: 100% (30 min) TOC removal: 85% (300 min)	[56]
FeCu	[Catalyst]: 100 mg/L; [H_2O_2]: 6 M; [Phenol]: 35 mg/L; pH: 4.0; room temperature	Phenol removal: 100% (30 min)	[57]
$Fe_3O_4/FeAl_2O_4$	PEO coating; [Catalyst]:35 mg/L; [H_2O_2]:6.0 mM; [Phenol]: 35 mg/L; pH: 4.0; T: 30 °C	Phenol removal: 100% (50 min)	[53]
Fe^0/Fe_3O_4-RGO	[Catalyst]: 1 g/L; [H_2O_2]: 5.0 mM; [Phenol]: 50 mg/L; pH: 3.0; T: 25 °C	Phenol removal: 100% (30 min)	[54]
Dendritic Fe^0	[Catalyst]: 100 mg/L; [H_2O_2]: 6.0 mM; [Phenol]: 35 mg/L; pH: 4.0; T: 30 °C	Phenol removal: 90% (15 min)	[55]
FeOCl/SBA-15	[Catalyst]: 200 mg/L; [H_2O_2]: 14.70 mM; [Phenol]: 100 mg/L; pH: 4.5; T: 40 °C	Phenol removal: 100% (15 min)	[58]
$SO_4{}^{2-}$–Fe_3O_4/FeS	TC4 coating; [Catalyst]: 20 g/L; [H_2O_2]: 6.0 mM; [Phenol]: 35 ppm; pH: 7.0; T: 30 °C	Phenol removal: 100% (3 min)	[59]
Fe^0@SiO_2	[Catalyst]: 1.08 g L^{-1}; [H_2O_2]: 120 mM; [Phenol]: 100 ppm; pH: 5.6; T: 60 °C	Phenol removal: 99.9% (45 min); TOC removal: 81% (60 min)	[60]

Several common aromatic pollutants, such as catechol, resorcinol and o-nitrophenol (ONP), were selected to evaluate the activity of the ZVI/Mn-C-31 catalyst under a neutral pH. The catalyst had good degradation activity for these pollutants. As shown in Figure 8, all three aromatic pollutants could be removed in 5 min, and a COD removal efficiency of 46%, 60% and 49% for catechol, resorcinol and o-nitrophenol, respectively, could be achieved, suggesting that the ZVI/Mn-C-31/H_2O_2 system possessed a wide usability for most common phenolic organics. The nonselective catalytic degradation process is of greater importance to practical applications in removing organic pollutants.

(**a**)　　　　　　　　　　　　　　　　　　　　　　(**b**)
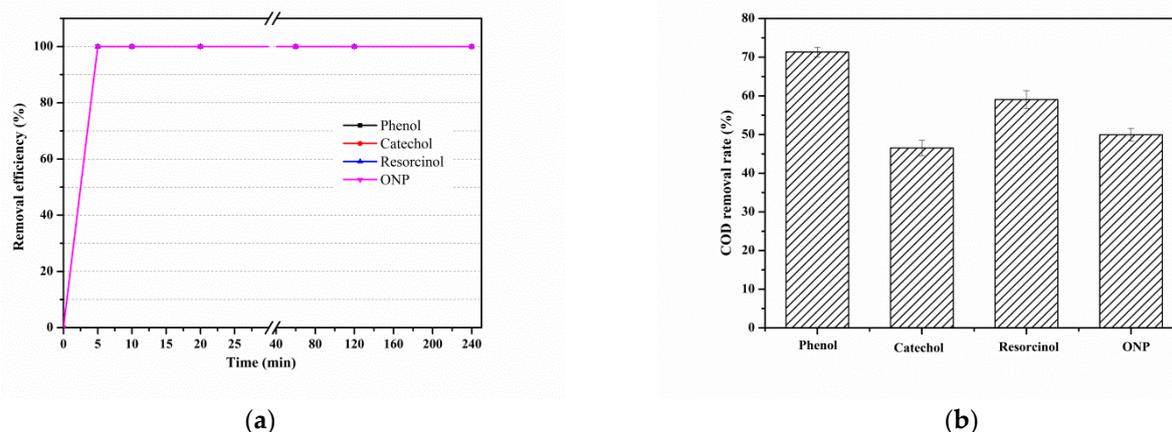
Figure 8. Effect of organic species on (**a**) the degradation of different organics and (**b**) COD removal (Conditions: [ZVI/Mn-C] = 2 g/L, [Pollutants] = 100 mg/L, [H_2O_2] = 0.2 mol/L, initial pH = 7).

The recycle test was performed under a neutral pH in the Fenton-like reaction for the phenol degradation to evaluate the stability of the ZVI/Mn-C-31 catalyst (Figure 9). After being calcined again at 850 °C in nitrogen for 4 h, the recycling catalyst could be reused three times without changing its removal efficiency and the phenol removal decreased from 100% to 80% in the fourth reaction within 5 min (Figure 9). These results demonstrated that this catalyst was essentially stable in this degradation reaction. Commonly, the activity loss of a heterogeneous catalyst results from the adsorption of intermediates on the catalysts and the poor dispersion of active component of catalyst [61,62]. The SEM image of the used ZVI/Mn-C-31 was also depicted and compared with fresh catalyst to evaluate its stability. As shown in Figure 10, the spherical ZVI nanoparticles in ZVI/Mn-C-31 after four successive cycles showed severe agglomeration, which might be responsible for the decrease in activity.
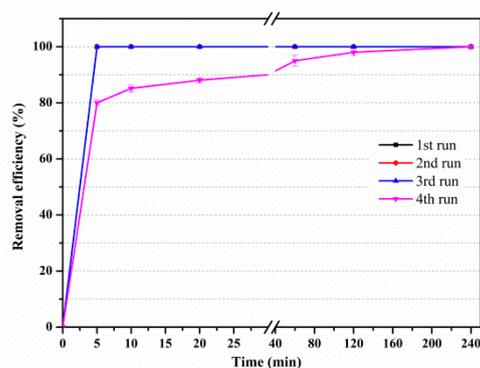

Figure 9. The catalytic stability of the ZVI/Mn-C-31 catalyst in the Fenton-like reaction for the phenol degradation (conditions: [ZVI/Mn-C-31] = 2 g/L, [phenol] = 100 mg/L, [H_2O_2] = 0.2 mol/L, initial pH = 7).
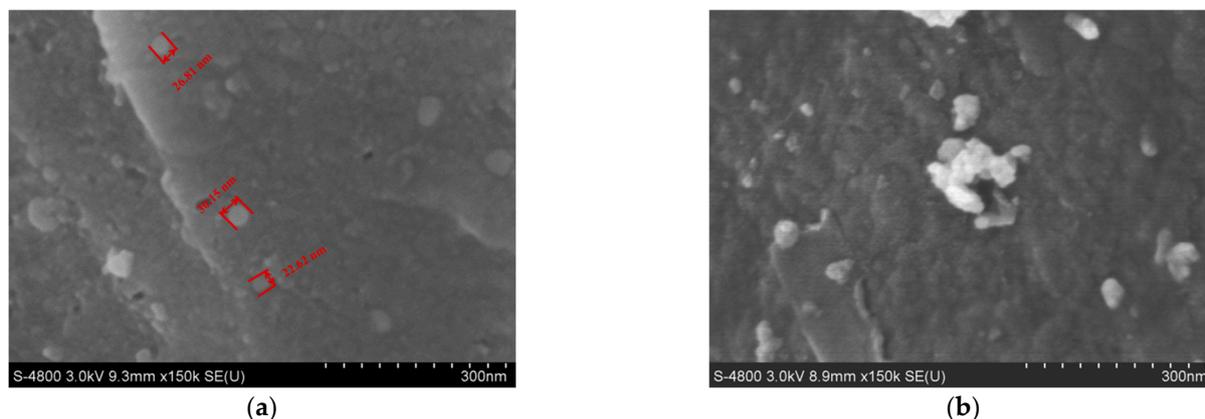
Figure 10. SEM images of ZVI/Mn-C-31 (**a**) before (**b**) after four reactions.
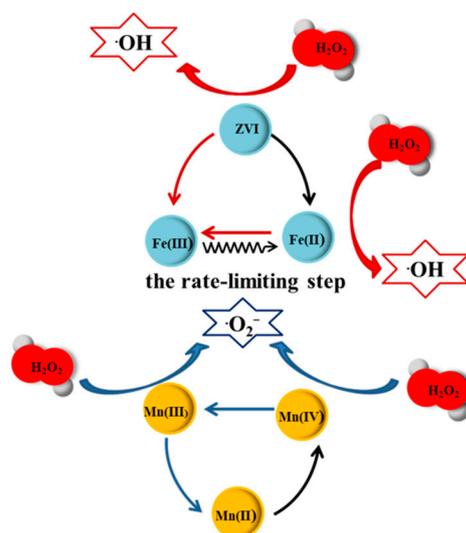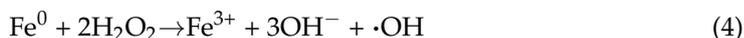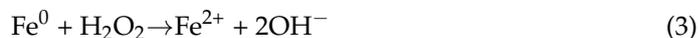
2.3. Mechanism Analysis

In order to identify the reactive species derived from the ZVI/Mn-C Fenton-like process, 2-propanol and chloroform were used as scavengers for $\cdot OH$ and $\cdot O_2^-$, respectively. The reaction was inhibited significantly after adding 2-propanol, while the addition of the $\cdot O_2^-$ scavenger chloroform resulted in a slight decline of the phenol removal (Figure 11). The results suggested that the degradation of phenol can be attributed to the generation of $\cdot OH$ assisted by $\cdot O_2^-$ in this Fenton-like process. With the participation of 2-propanol and chloroform, the degradation efficiency decreased to 36.5% and 93.4%, respectively. It was obvious that the $\cdot OH$ radicals played the leading role during the phenol degradation process when compared to the O_2^- radicals.
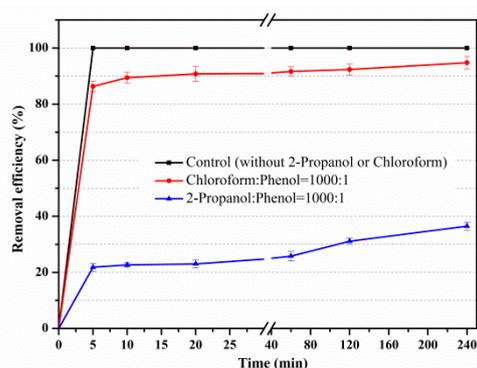
Figure 11. Effect of 2-propanol and chloroform on the degradation of phenol in aqueous solutions by the ZVI/Mn-C-31 Fenton-like process (conditions: [ZVI/Mn-C-31] = 2 g/L, [phenol] = 100 mg/L, [H_2O_2] = 0.2 mol/L, initial pH = 7).

To explain the special behavior of these bimetallic s samples, the reaction mechanism should be investigated. Because of the outstanding electron conductive properties, carbon species were considered to be effective carriers for the redox cycles [63]. The proposed mechanism of this Fenton-like system employing a spherical ZVI/Mn-C bimetallic catalyst is shown in Figure 12. ZVI usually acted as an electron donor (reducing agent), reacting with dissolved O_2 and H_2O_2 in the aqueous solution to generate effective sources of strong oxidizing substances OH (Equations (1) and (2)) [64,65]. ZVI can be also effectively oxidized by H_2O_2 during the Fenton-like reaction process (Equations (3) and (4)) [66]. Subsequently, the as-produced Fe^{2+} participated in the generation of $\cdot OH$, which was responsible for degrading the target pollutants (Equation (6)) [67]. With the existence of H_2O_2, the rate-limiting step of the heterogeneous Fenton reaction is widely believed to be the conversion

of Fe^{3+} to Fe^{2+} [68,69]. In this ZVI-driven Fenton-like reaction, ZVI, as a strong reducing agent, provided an additional path for the iron circulation (Equations (5), (7) and (8)) [70].

$$Fe^0 + 2H_2O \rightarrow Fe^{2+} + H_2 + 2OH^- \tag{1}$$

$$Fe^0 + O_2 + 2H^+ \rightarrow Fe^{2+} + H_2O_2 \tag{2}$$

$$Fe^0 + H_2O_2 \rightarrow Fe^{2+} + 2OH^- \tag{3}$$

$$Fe^0 + 2H_2O_2 \rightarrow Fe^{3+} + 3OH^- + \cdot OH \tag{4}$$

$$2Fe^{3+} + Fe^0 \rightarrow 3Fe^{2+} \tag{5}$$

$$Fe^{2+} + H_2O_2 \rightarrow Fe^{3+} + OH^- + \cdot OH \tag{6}$$

$$Fe^{3+} + H_2O_2 \rightarrow Fe^{2+} + 2H^+ + \cdot O_2^- \tag{7}$$

$$Fe^{3+} + \cdot O_2^- \rightarrow Fe^{2+} + O_2 \tag{8}$$

Figure 12. Proposed mechanism for the Fenton-like system over ZVI/Mn-C bimetallic catalyst.

Superoxide radicals can be generated from the $MnO–H_2O_2$ system according to previous reports [35,71]. The interaction between Mn^{2+} and H_2O_2 played a key role in the organic oxidation process especially under neutral conditions (Equation (9)). Mn^{4+} and Mn^{3+} can be obtained by reduction reactions involving H_2O_2 and then generated $\cdot O_2^-$ in the following reactions (Equations (10) and (11)), thereby the conversion rate of ferric iron to ferrous iron was accelerated (Equation (8)). Based on the above analysis, it can be concluded that the reaction activity can be effectively promoted by adding manganese in an appropriate amount. However, it should also be noticed that with excessive manganese, hydrogen peroxide would be consumed quickly resulting in less hydroxyl radicals (Equations (9) and (11)). Therefore, the bimetallic Fenton-like reaction greatly benefitted from a proper Fe/Mn ratio due to the synergistic effects of ZVI and MnO, which is consistent with the XPS results.

$$Mn^{2+} + H_2O_2 \rightarrow Mn^{4+} + 2OH^- \tag{9}$$

$$Mn^{4+} + H_2O_2 \rightarrow Mn^{3+} + 2H^+ + \cdot O_2^- \tag{10}$$

$$Mn^{3+} + H_2O_2 \rightarrow Mn^{2+} + 2H^+ + \cdot O_2^- \tag{11}$$
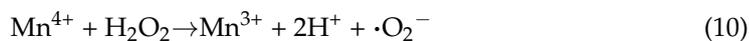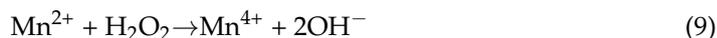
3. Materials and Methods

3.1. Materials

Sodium hydroxide, phenol and the formaldehyde solution (37 wt %) were purchased from Tianjin Jiangtian Chemical Reagent Co., Ltd. (Tianjin, China). Ammonium alginate (ALG) was purchased from Shandong Mingyue Seaweed Group. Ferric chloride hexahydrate ($FeCl_3 \cdot 6H_2O$), manganese (II) chloride tetrahydrate ($MnCl_2 \cdot 4H_2O$), polyethylene (PE), hydrogen peroxide (H_2O_2) were obtained from Tianjin Kemiou Chemical Reagent Co., Ltd. (Tianjin, China). All reagents were used as received without further purification.

3.2. Preparation of ZVI/Mn-C Spheres

The millimeter-scale carbon spheres were prepared via the ammonium alginate assisted sol–gel method. First, sodium hydroxide, phenol and formaldehyde were added to a 100 mL round bottom flask in a mass ratio of 1:5:9, respectively. The resulting mixture was sealed and heated to 95 °C under vigorous stirring for 120 min. Then, the obtained water-soluble PF, PE and ALG solution (2 wt %) were mixed uniformly in a certain proportion. The suspension was dropped slowly by a syringe into gel solutions with different molar ratios of Fe^{3+}/Mn^{2+}, and the semirigid beads were formed instantaneously. The as-prepared wet beads were soaked for 12 h in solution and filtered. Finally, the samples were dried at room temperature and 120 °C for 48 h and 12 h, respectively, and calcined at 850 °C for 4 h in a high purity N_2 atmosphere. Five ZVI/Mn-C spheres were synthesized individually, and the preparation details and labels are listed in Table 3.

Table 3. The preparation details and labels of the ZVI/Mn-C spheres.

Sample	$c(Fe^{3+})/mol \cdot L^{-1}$	$c(Mn^{2+})/mol \cdot L^{-1}$	$c(Fe^{3+})/c(Mn^{2+})$
ZVI-C	0.40	0	-
ZVI/Mn-C-31	0.30	0.10	3:1
ZVI/Mn-C-11	0.20	0.20	1:1
ZVI/Mn-C-13	0.10	0.30	1:3
Mn-C	0	0.40	0

3.3. Characterization

X-ray diffraction (XRD) characterizations were carried out on a Bruker AXS D8 powder X-ray diffractometer with graphite monochromatic Cu-Kα radiation at 40 kV and 200 mA. The Raman spectra were recorded with a LabRAM HR Evolution confocal Raman microscope equipped with imaging system using an ion laser operating at 532 nm with a charge-coupled device detector. Transmission electron microscope (TEM) images were obtained with a JEOL JEM-2100F field emission electron microscope at 200 kV. X-ray photoelectron spectroscopy (XPS) measurements were performed on a Thermo SCIENTIFIC ESCALAB 250Xi spectrometer with all binding energies calibrated to the C 1 s peak at 284.8 eV. The low temperature N_2 adsorption–desorption test was performed on an automated analyzer (QUA211007, Quantachrome, Boynton Beach, FL, USA). The ultimate mechanical strength of the spherical activated carbon was tested using a YHCK-2A particle strength determinator to calculate the ultimate mechanical strength of the spheres. Scanning electron microscope (SEM) images were obtained by using s-4800 at an accelerating voltage of 3 kV.

3.4. Other Analysis

The aqueous phenol concentration was measured by 4-aminoantipyrine direct photometric method using a PerkinElmer Lambda 750 UV-visible spectrophotometer at a wavelength of 510 nm. The conversion of COD was determined by the potassium dichromate oxidation method. Specifically, all samples were filtered by 0.45 μm BOJIN Luer syringe filters.

4. Conclusions

In summary, ZVI/Mn-C spheres were successfully fabricated through the ammonium-alginate-assisted sol–gel method, characterized by XRD, TEM, XPS and Raman spectroscopy and tested for the degradation of phenol by the Fenton-like reaction. The results showed that the ZVI and MnO particles embedded in the carbon layer had a good dispersion and small size. Among all catalysts, ZVI/Mn-C-31 exhibited the highest removal rates of phenol and COD due to the optimal synergistic effects between ZVI and MnO. The ZVI/Mn-C-31/H_2O_2 system also possessed good activities for degrading catechol, resorcinol and ONP, and all pollutants could be completely removed under neutral pH within 5 min. With MnO assisting, the Fenton-like process maintained sufficient degradation rate even in an extended pH range of 4.0–8.0. Furthermore, it was illustrated through radicals-scavenging experiments that ·OH was primarily responsible for the degradation. It means that the catalyst could be used to degrade different organic pollutants. On the other hand, the intermediates of the phenol oxidation could be further detected in the future work, which would be helpful in understanding the mechanism and degradation pathway of pollutants by ZVI/Mn-C bimetallic catalysts. In conclusion, the ZVI/Mn-C catalysts are quite practical in the field of water treatment and deserve a broader application.

Data Availability Statement: Data are contained within the article.

References

1. Babuponnusami, A.; Muthukumar, K. Advanced oxidation of phenol: A comparison between Fenton, electro-Fenton, sono-electro-Fenton and photo-electro-Fenton processes. *Chem. Eng. J.* **2012**, *183*, 1–9. [CrossRef]
2. Niu, S.P.; Sun, F. Application of Immobilized Microorganisms Technology for Wastewater Treatment. In Proceedings of the International Workshop on Diffuse Pollution-Management Measures and Control Technique, Huainan, China, 27–29 October 2010; Anhui University of Science and Technology: Huainan, China, 2010; p. 359.
3. He, J.; Zhang, W. An Optimized Method Using Light Enhanced Fenton to Treat Highly Toxic Phenol Wastewater. *Asian J. Chem.* **2013**, *25*, 4583–4587. [CrossRef]
4. Asgari, G.; Feradmal, J.; Poormohammadi, A.; Sadrnourmohamadi, M.; Akbari, S. Taguchi optimization for the removal of high concentrations of phenol from saline wastewater using electro-Fenton process. *Desalination Water Treat.* **2016**, *57*, 27331–27338. [CrossRef]
5. Cao, C.Y.; Meng, L.K.; Zhao, Y.H. Adsorption of phenol from wastewater by organo-bentonite. *Desalination Water Treat.* **2014**, *52*, 3504–3509. [CrossRef]
6. Tian, R.; Wang, F.C.; Yu, C.M.; Li, X.G. Research of advanced oxidation treatment of organic wastewater, 3rd. In Proceedings of the International Conference on Energy, Environment and Sustainable Development (EESD 2013), Shanghai, China, 12–13 November 2013; pp. 1621–1625.
7. Verma, M.; Haritash, A.K. Degradation of amoxicillin by Fenton and Fenton-integrated hybrid oxidation processes. *J. Environ.* **2019**, *7*, 102886. [CrossRef]
8. Rodrigues-Silva, F.; Lemos, C.R.; Naico, A.A.; Fachi, M.M.; do Amaral, B.; de Paula, V.C.S.; Rampon, D.S.; Beraldi-Magalhaes, F.; Prola, L.D.T.; Pontarolo, R.; et al. Study of isoniazid degradation by Fenton and photo-Fenton processes, by-products analysis and toxicity evaluation. *J. Photochem. Photobiol. A Chem.* **2022**, *425*, 113671. [CrossRef]
9. Kulaksiz, E.; Kayan, B.; Gozmen, B.; Kalderis, D.; Oturan, N.; Oturan, M.A. Comparative degradation of 5-fluorouracil in aqueous solution by using H2O2-modified subcritical water, photocatalytic oxidation and electro-Fenton processes. *Environ. Res.* **2022**, *204*, 111898. [CrossRef]
10. Cheng, Z.Y.; Li, S.P.; Nguyen, T.T.; Gao, X.; Luo, S.Y.; Guo, M.H. Biochar loaded on MnFe2O4 as Fenton catalyst for Rhodamine B removal: Characterizations, catalytic performance, process optimization and mechanism. *Colloids Surf. A Physicochem. Eng. Asp.* **2021**, *631*, 127651. [CrossRef]

11. Wang, M.W.; Zhao, Z.Q.; Zhang, Y.B. Sustainable Strategy for Enhancing Anaerobic Digestion of Waste Activated Sludge: Driving Dissimilatory Iron Reduction with Fenton Sludge. *ACS Sustain. Chem. Eng.* **2018**, *6*, 2220–2230. [CrossRef]

12. Gao, L.H.; Cao, Y.J.; Wang, L.Z.; Li, S.L. A review on sustainable reuse applications of Fenton sludge during wastewater treatment. *Front. Environ. Sci. Eng.* **2022**, *16*, 77. [CrossRef]

13. Meijide, J.; Dunlop, P.S.M.; Pazos, M.; Sanroman, M.A. Heterogeneous Electro-Fenton as "Green" Technology for Pharmaceutical Removal: A Review. *Catalysts* **2021**, *11*, 85. [CrossRef]

14. Ding, J.; Jiang, M.; Zhao, G.S.; Wei, L.L.; Wang, S.N.; Zhao, Q.L. Treatment of leachate concentrate by electrocoagulation coupled with electro-Fenton-like process: Efficacy and mechanism. *Sep. Purif. Technol.* **2021**, *255*, 117668. [CrossRef]

15. Matira, E.M.; Chen, T.C.; Lu, M.C.; Dalida, M.L.P. Degradation of dimethyl sulfoxide through fluidized-bed Fenton process. *J. Hazard. Mater.* **2015**, *300*, 218–226. [CrossRef] [PubMed]

16. Rahimi, S.M.; Al-Musawi, T.J.; Arghavan, F.S.; Nasseh, N. Mechanism and efficiency of metronidazole removal via adsorption and heterogeneous Fenton reaction using FeNi3 nanoparticles. *Desalination Water Treat.* **2021**, *234*, 136–146. [CrossRef]

17. Wang, Y.T.; Tu, C.H.; Lin, Y.S. Application of Graphene and Carbon Nanotubes on Carbon Felt Electrodes for the Electro-Fenton System. *Materials* **2019**, *12*, 1698. [CrossRef]

18. Oliveira, W.L.; Ferreira, M.A.; Mourao, H.; Pires, M.J.M.; Ferreira, V.; Gorgulho, H.F.; Cipriano, D.F.; Freitas, J.C.C.; Mastelaro, V.R.; Nascimento, O.R.; et al. Heterogeneous Fenton-like surface properties of oxygenated graphitic carbon nitride. *J. Colloid Interface Sci.* **2021**, *587*, 479–488. [CrossRef]

19. Garcia, J.C.; Pedroza, A.M.; Daza, C.E. Magnetic Fenton and Photo-Fenton-Like Catalysts Supported on Carbon Nanotubes for Wastewater Treatment. *Water Air Soil Pollut.* **2017**, *228*, 246. [CrossRef]

20. Cleveland, V.; Bingham, J.P.; Kan, E. Heterogeneous Fenton degradation of bisphenol A by carbon nanotube-supported Fe3O4. *Sep. Purif. Technol.* **2014**, *133*, 388–395. [CrossRef]

21. Bury, N.A.; Mumford, K.A.; Stevens, G.W. The electro-Fenton regeneration of Granular Activated Carbons: Degradation of organic contaminants and the relationship to the carbon surface. *J. Hazard. Mater.* **2021**, *416*, 125792. [CrossRef]

22. Li, W.H.; Wu, X.F.; Li, S.D.; Tang, W.; Chen, Y.F. Magnetic porous Fe3O4/carbon octahedra derived from iron-based metal-organic framework as heterogeneous Fenton-like catalyst. *Appl. Surf. Sci.* **2018**, *436*, 252–262. [CrossRef]

23. Minella, M.; Bertinetti, S.; Hanna, K.; Minero, C.; Vione, D. Degradation of ibuprofen and phenol with a Fenton-like process triggered by zero-valent iron (ZVI-Fenton). *Environ. Res.* **2019**, *179*, 108750. [CrossRef] [PubMed]

24. Dos Santos, N.O.; Teixeira, L.A.C.; Spadotto, J.C.; Campos, L.C. A simple ZVI-Fenton pre-oxidation using steel-nails for NOM degradation in water treatment. *J. Water Process Eng.* **2021**, *43*, 102230. [CrossRef]

25. Donadelli, J.A.; Caram, B.; Kalaboka, M.; Kapsi, M.; Sakkas, V.A.; Carlos, L.; Einschlag, F.S.G. Mechanisms of 4-phenylazophenol elimination in micro- and nano-ZVI assisted-Fenton systems. *J. Environ. Chem. Eng.* **2020**, *8*, 103624. [CrossRef]

26. Huang, Y.H.; Tang, C.L.; Zeng, H. Removing molybdate from water using a hybridized zero-valent iron/magnetite/Fe(II) treatment system. *Chem. Eng. J.* **2012**, *200*, 257–263. [CrossRef]

27. Chen, S.; Li, Z.X.; Belver, C.; Gao, G.L.; Guan, J.; Guo, Y.G.; Li, H.; Ma, J.; Bedia, J.; Wojtowicz, P. Comparison of the behavior of ZVI/carbon composites from both commercial origin and from spent Li-ion batteries and mill scale for the removal of ibuprofen in water. *J. Environ. Manag.* **2020**, *264*, 110480. [CrossRef] [PubMed]

28. Du, Y.F.; Dai, M.; Naz, I.; Hao, X.Y.; Wei, X.X.; Rong, R.; Peng, C.S.; Ali, I. Carbothermal reduction synthesis of zero-valent iron and its application as a persulfate activator for ciprofloxacin degradation. *Sep. Purif.Technol.* **2021**, *275*, 119201. [CrossRef]

29. Hussain, S.; Aneggi, E.; Goi, D.; Trovarelli, A. Bimetallic Cu/Fe Catalysts for Ibuprofen Mineralization. *Catalysts* **2021**, *11*, 1383. [CrossRef]

30. Li, J.C.; Li, X.H.; Han, J.D.; Meng, F.S.; Jiang, J.Y.; Li, J.; Xu, C.L.; Li, Y. Mesoporous bimetallic Fe/Co as highly active heterogeneous Fenton catalyst for the degradation of tetracycline hydrochlorides. *Sci. Rep.* **2019**, *9*, 15820. [CrossRef]

31. Li, X.F.; Liu, W.P.; Ma, J.Q.; Wen, Y.Z.; Wu, Z.C. High catalytic activity of magnetic FeOx/NiOy/SBA-15: The role of Ni in the bimetallic oxides at the nanometer level. *Appl. Catal. B Environ.* **2015**, *179*, 239–248. [CrossRef]

32. Oruc, Z.; Ergut, M.; Uzunoglu, D.; Ozer, A. Green synthesis of biomass-derived activated carbon/Fe-Zn bimetallic nanoparticles from lemon (*Citrus limon* (L.) *Burm.* f.) wastes for heterogeneous Fenton-like decolorization of Reactive Red 2. *J. Environ. Chem. Eng.* **2019**, *7*, 103231. [CrossRef]

33. Santos, B.L.C.; Parpot, P.; Soares, O.; Pereira, M.F.R.; Rombi, E.; Fonseca, A.M.; Neves, I.C. Fenton-Type Bimetallic Catalysts for Degradation of Dyes in Aqueous Solutions. *Catalysts* **2021**, *11*, 32. [CrossRef]

34. Sun, Q.; Liu, M.; Li, K.; Han, Y.; Zuo, Y.; Chai, F.; Song, C.; Zhang, G.; Guo, X. Synthesis of Fe/M (M = Mn, Co, Ni) bimetallic metal organic frameworks and their catalytic activity for phenol degradation under mild conditions. *Inorg. Chem. Front.* **2017**, *4*, 144–153. [CrossRef]

35. Li, Y.; Sun, J.; Sun, S.P. Mn^{2+}-mediated homogeneous Fenton-like reaction of Fe(III)-NTA complex for efficient degradation of organic contaminants under neutral conditions. *J. Hazard. Mater.* **2016**, *313*, 193–200. [CrossRef] [PubMed]

36. Li, L.; Deng, Y.; Ai, J.; Li, L.; Liao, G.; Xu, S.; Wang, D.; Zhang, W. Fe/Mn loaded sludge-based carbon materials catalyzed oxidation for antibiotic degradation: Persulfate vs H$_2$O$_2$ as oxidant. *Sep. Purif. Technol.* **2021**, *263*, 118409. [CrossRef]

37. Peleyeju, M.G.; Mgedle, N.; Viljoen, E.L.; Scurrel, M.S.; Ray, S.C. Irradiation of Fe–Mn@SiO2 with microwave energy enhanced its Fenton-like catalytic activity for the degradation of methylene blue. *Res. Chem. Intermed.* **2021**, *47*, 4213–4226. [CrossRef]

38. Wang, X.; Xin, C.; Shi, C.; Dong, A.; Wang, K. Simple Preparation of Spherical Activated Carbon with Mesoporous Structure from Phenolic Resol and Associated Catalytic Performance in Isobutane Dehydrogenation. *Trans. Tianjin Univ.* **2018**, *24*, 351–360. [CrossRef]

39. Pani, S.; Singh, S.K.; Mohapatra, B.K. Synthesis and Characterization of MnO Nano-particles Using Thermal Plasma Technique. *Trans. Indian Inst. Met.* **2019**, *72*, 65–71. [CrossRef]

40. Hadzic, B.; Vasic, B.; Matovic, B.; Kuryliszyn-Kudelska, I.; Dobrowolski, W.; Romcevic, M.; Romcevic, N. Influence of laser-induced heating on MnO nanoparticles. *J. Raman Spectrosc.* **2018**, *49*, 817–821. [CrossRef]

41. Zhang, K.J.; Han, P.X.; Gu, L.; Zhang, L.X.; Liu, Z.H.; Kong, Q.S.; Zhang, C.J.; Dong, S.M.; Zhang, Z.Y.; Yao, J.H.; et al. Synthesis of Nitrogen-Doped MnO/Graphene Nanosheets Hybrid Material for Lithium Ion Batteries. *ACS Appl. Mater. Interfaces* **2012**, *4*, 658–664. [CrossRef]

42. Sewwandi, K.A.H.S.; Nitisoravut, R. Nano zero valent iron embedded on chitosan for enhancement of biohydrogen production in dark fermentation. *Energy Rep.* **2020**, *6*, 392–396. [CrossRef]

43. Sun, Y.P.; Li, X.Q.; Cao, J.; Zhang, W.X.; Wang, H.P. Characterization of zero-valent iron nanoparticles. *Adv. Colloid Interface Sci.* **2006**, *120*, 47–56. [CrossRef] [PubMed]

44. Yang, K.; Xu, J.; Zhang, M.; Lin, D. Re-recognizing micro locations of nanoscale zero-valent iron in biochar using C-TEM technique. *Sci. Rep.* **2021**, *11*, 5037. [CrossRef] [PubMed]

45. Pandey, B.K.; Shahi, A.K.; Gopal, R. Synthesis, optical properties and growth mechanism of MnO nano structures. *Appl. Surf. Sci.* **2013**, *283*, 430–437. [CrossRef]

46. Segura, Y.; Martínez, F.; Melero, J.A.; Fierro, J.L.G. Zero valent iron (ZVI) mediated Fenton degradation of industrial wastewater: Treatment performance and characterization of final composites. *Chem. Eng. J.* **2015**, *269*, 298–305. [CrossRef]

47. Pradhan, A.C.; Nanda, B.; Parida, K.M.; Rao, G.R. Fabrication of the Mesoporous Fe@MnO$_2$NPs-MCM-41 Nanocomposite: An Efficient Photocatalyst for Rapid Degradation of Phenolic Compounds. *J. Phys. Chem. C* **2015**, *119*, 14145–14159. [CrossRef]

48. Wang, A.Q.; Chen, Z.; Zheng, Z.K.; Xu, H.; Wang, H.; Hu, K.; Yan, K. Remarkably enhanced sulfate radical-based photo-Fenton-like degradation of levofloxacin using the reduced mesoporous MnO@MnOx microspheres. *Chem. Eng. J.* **2020**, *379*, 122340. [CrossRef]

49. Zhou, Y.; Xiao, B.; Liu, S.Q.; Meng, Z.D.; Chen, Z.G.; Zou, C.Y.; Liu, C.B.; Chen, F.; Zhou, X. Photo-Fenton degradation of ammonia via a manganese-iron double-active component catalyst of graphene-manganese ferrite under visible light. *Chem. Eng. J.* **2016**, *283*, 266–275. [CrossRef]

50. Niveditha, S.V.; Gandhimathi, R. Flyash augmented Fe$_3$O$_4$ as a heterogeneous catalyst for degradation of stabilized landfill leachate in Fenton process. *Chemosphere* **2020**, *242*, 125189. [CrossRef]

51. Siddiqui, S.; Keswani, M.; Brooks, B.; Fuerst, A.; Raghavan, S. A study of hydrogen peroxide decomposition in ammonia-peroxide mixtures (APM). *Microelectron. Eng.* **2013**, *102*, 68–73. [CrossRef]

52. Ma, J.; Yang, M.X.; Yu, F.; Chen, J.H. Easy solid-phase synthesis of pH-insensitive heterogeneous CNTs/FeS Fenton-like catalyst for the removal of antibiotics from aqueous solution. *J. Colloid Interface Sci.* **2015**, *444*, 24–32. [CrossRef]

53. Wang, J.K.; Yao, Z.P.; Yang, M.; Wang, Y.J.; Xia, Q.X.; Jiang, Z.H. A Fe$_3$O$_4$/FeAl$_2$O$_4$ composite coating via plasma electrolytic oxidation on Q235 carbon steel for Fenton-like degradation of phenol. *Environ. Sci. Pollut. Res.* **2016**, *23*, 14927–14936. [CrossRef] [PubMed]

54. Wang, P.L.; Zhou, X.; Zhang, Y.G.; Yang, L.P.; Zhi, K.K.; Wang, L.L.; Zhang, L.T.; Guo, X.F. Unveiling the mechanism of electron transfer facilitated regeneration of active Fe2+ by nano-dispersed iron/graphene catalyst for phenol removal. *RSC Adv.* **2017**, *7*, 26983–26991. [CrossRef]

55. Xia, Q.X.; Jiang, Z.H.; Wang, J.K.; Yao, Z.P. A facile preparation of hierarchical dendritic zero-valent iron for Fenton-like degradation of phenol. *Catal. Commun.* **2017**, *100*, 57–61. [CrossRef]

56. Wang, W.M.; Song, J.; Han, X. Schwertmannite as a new Fenton-like catalyst in the oxidation of phenol by H2O2. *J. Hazard. Mater.* **2013**, *262*, 412–419. [CrossRef]

57. Xia, Q.X.; Zhang, D.J.; Yao, Z.P.; Jiang, Z.H. Revealing the enhancing mechanisms of Fe-Cu bimetallic catalysts for the Fenton-like degradation of phenol. *Chemosphere* **2022**, *289*, 133195. [CrossRef]

58. Yang, X.J.; Tian, P.F.; Zhang, X.M.; Yu, X.; Wu, T.; Xu, J.; Han, Y.F. The Generation of Hydroxyl Radicals by Hydrogen Peroxide Decomposition on FeOCl/SBA-15 Catalysts for Phenol Degradation. *AIChE J.* **2015**, *61*, 166–176. [CrossRef]

59. Zhang, X.; Wang, J.K.; Yao, Z.P.; Chen, C.J.; Zhou, Y.; Jiang, Z.H. Synthesis of the SO$_4$$^{2-}$-Fe$_3O_4$/FeS coating catalyst on a TC4 titanium alloy for the enhanced Fenton-like degradation of phenol. *New J. Chem.* **2021**, *45*, 1516–1524. [CrossRef]

60. Liu, C.; Li, J.; Qi, J.; Wang, J.; Luo, R.; Shen, J.; Sun, X.; Han, W.; Wang, L. Yolk-shell Fe^0@SiO$_2$ nanoparticles as nanoreactors for fenton-like catalytic reaction. *ACS Appl. Mater. Interfaces* **2014**, *6*, 13167–13173. [CrossRef]

61. Panjwani, M.K.; Wang, Q.; Ma, Y.; Lin, Y.; Xiao, F.; Yang, S. High degradation efficiency of sulfamethazine with the dual-reaction-center Fe–Mn–SiO$_2$ Fenton-like nanocatalyst in a wide pH range. *Environ. Sci. Nano* **2021**, *8*, 2204–2213. [CrossRef]

62. Gao, P.; Chen, X.J.; Hao, M.J.; Xiao, F.; Yang, S.X. Oxygen vacancy enhancing the Fe$_2$O$_3$-CeO$_2$ catalysts in Fenton-like reaction for the sulfamerazine degradation under O$_2$ atmosphere. *Chemosphere* **2019**, *228*, 521–527. [CrossRef]

63. Ahsan, M.A.; Puente Santiago, A.R.; Rodriguez, A.; Maturano-Rojas, V.; Alvarado-Tenorio, B.; Bernal, R.; Noveron, J.C. Biomass-derived ultrathin carbon-shell coated iron nanoparticles as high-performance tri-functional HER, ORR and Fenton-like catalysts. *J. Clean. Prod.* **2020**, *275*, 124141. [CrossRef]

64. Aramyan, S.M. Advances in Fenton and Fenton Based Oxidation Processes for Industrial Effluent Contaminants Control-A Review. *Int. J. Environ. Sci. Nat. Resour.* **2017**, *2*, 1–18. [CrossRef]

65. He, J.; Yang, X.; Men, B.; Wang, D. Interfacial mechanisms of heterogeneous Fenton reactions catalyzed by iron-based materials: A review. *J. Environ. Sci.* **2016**, *39*, 97–109. [CrossRef] [PubMed]

66. Rosales, E.; Sanromán, M.Á.; Dias-Ferreira, C. Green zero-valent iron nanoparticles synthesized using herbal extracts for degradation of dyes from wastewater. *Desalination Water Treat.* **2017**, *92*, 159–167. [CrossRef]

67. Raman, C.D.; Kanmani, S. Textile dye degradation using nano zero valent iron: A review. *J. Environ. Manag.* **2016**, *177*, 341–355. [CrossRef] [PubMed]

68. Wang, J.; Tang, J. Fe-based Fenton-like catalysts for water treatment: Catalytic mechanisms and applications. *J. Mol. Liq.* **2021**, *332*, 115755. [CrossRef]

69. Rigg, T.; Taylor, W.; Weiss, J. The Rate Constant of the Reaction between Hydrogen Peroxide and Ferrous Ions. *J. Chem. Phys.* **1954**, *22*, 575–577. [CrossRef]

70. Zhou, T.; Li, Y.; Ji, J.; Wong, F.-S.; Lu, X. Oxidation of 4-chlorophenol in a heterogeneous zero valent iron/H2O2 Fenton-like system: Kinetic, pathway and effect factors. *Sep. Purif. Technol.* **2008**, *62*, 551–558. [CrossRef]

71. Baral, S.; Lume-Pereira, C.; Janata, E.; Henglein, A. Chemistry of colloidal manganese dioxide. 2. Reaction with superoxide anion (O_2^-) and hydrogen peroxide (pulse radiolysis and stop flow studies). *J. Phys. Chem.* **1985**, *89*, 5779–5783. [CrossRef]